Compressive Acquisition of Sparse Deflectometric Maps

Prasad Sudhakar, Laurent Jacques and Adriana Gonzalez
ELEN Department, ICTEAM
Université catholique de Louvain, Belgium.
Email: firstname.secondname@uclouvain.be

Xavier Dubois, Philippe Antoine and Luc Joannes
Lambda-X
Nivelles, Belgium.
Email: firstname.secondname@lambda-x.com

***Abstract*—Schlieren deflectometry aims at measuring deflections of light rays from transparent objects, which is subsequently used to characterize the objects. With each location on a smooth object surface a sparse deflection map (or spectrum) is associated. In this paper, we demonstrate the compressive acquisition and reconstruction of such maps, and the usage of deflection information for object characterization, using a schlieren deflectometer. To this end, we exploit the sparseness of deflection maps and we use the framework of spread spectrum compressed sensing. Further, at a second level, we demonstrate how to use the deflection information optimally to reconstruct the distribution of refractive index inside an object, by exploiting the sparsity of refractive index maps in gradient domain.**

I. Introduction

Schlieren deflectometry is a modality to measure the deflections undergone by light in a transparent object [1]. These deflections are used to characterize the properties of the transparent objects such as the surface curvature, distribution of the refractive index, etc. Unlike interferometry, deflectometry is insensitive to vibrations and hence is very attractive for industrial deployment (*e.g.*, for quality control).

Considering a thin transparent object with an incident parallel beam of light rays, as shown in Fig. 1(left). At each surface location $\boldsymbol{p}$, the function of our interest is a *deflection spectrum* $\tilde{s}_{\boldsymbol{p}}(\theta,\varphi) \in \mathbb{R}_+$, representing the flux of the light deviated in the direction (θ,φ), in a spherical coordinate system. These deflection spectra provide information about the curvature of the object, and hence it is interesting to study them.

For convenience, $\tilde{s}_{\boldsymbol{p}}$ is represented in this paper by its projection in the $\Pi_{\boldsymbol{p}} = \boldsymbol{e}_2\boldsymbol{e}_3$ plane, *i.e.*, according to the projected function $s_{\boldsymbol{p}}(r(\theta),\varphi) = \tilde{s}_{\boldsymbol{p}}(\theta,\varphi)$ with $r(\theta) = \tan\theta$. Moreover, the object surface is assumed sufficiently smooth for being parametrized by a projection of $\boldsymbol{p}$ in the same plane (on a arbitrary fixed origin), so that $\boldsymbol{p}$ is basically a 2-D vector.

An important feature of deflections is that for most objects (*e.g.*, with smooth surfaces), for any location $\boldsymbol{p}$, the flux is limited to range of angles and hence the deflection spectra therefore tend to be naturally *sparse* in plane $\Pi_{\boldsymbol{p}}$ or in some appropriate basis of this domain (*e.g.*, wavelets). Fig. 1(right) shows an example of a discretized deflection spectrum $s_{\boldsymbol{p}}$ for one location of a plano convex lens obtained using the setup described in Sec. II. The white spot in the image signifies that deflections occur at only a few angles (as governed by classical optics) and deflections elsewhere are negligible.

The optical setup described in Sec. II measures the deflection spectrum $s_{\boldsymbol{p}}$ for each location $\boldsymbol{p}$ indirectly by optical comparison with a certain number of programmable modulation patterns. Computationally, these optical comparisons are nothing but inner products between the deflection spectrum and the modulation patterns. By assuming an extreme case of the spectrum being a mere impulse, Phase Shifting Schlieren (PSS) method measures the deflection angles by using multiline phase shifted patterns in the SLM [2]. However, it is a limitation to ignore the richness of the deflection spectrum.

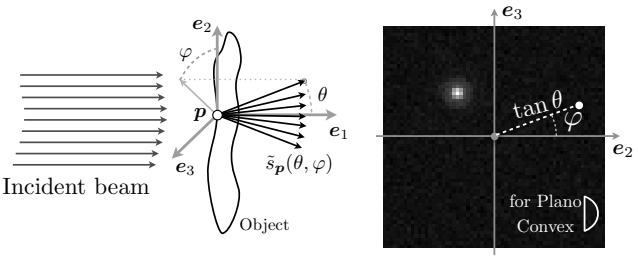

Fig. 1: Left, illustration of a deflection spectrum. Right, a typical (projected) deflection spectrum $s_{\boldsymbol{p}}$ for a plano convex lens of optical power 25.12D.

To this end, aided by the hindsight that each deflection spectra is sparse, we use the framework of *spread spectrum*[1] compressive sensing [3], described in Sec. III, to capture maximum information about the spectrum using relatively few modulation patterns, and then reconstruct the spectrum at each location by solving an inverse problem. In effect, each CCD pixel of our system behaves like a *single pixel camera* [4], but for deflection spectrum.

In Sec. IV, we present the numerical results of reconstructing deflection spectra from deflectometric measurements, after calibrating the system relative to its intrinsic noise. By making further assumptions about the spectra, we show in Sec. V how the deflection information can be obtained without explicit reconstruction of the spectra.

If the object contains regions of varying refractive index, then light undergoes deflections internally and at each surface location only the resultant deflection is measured. Therefore, the deflections provide indirect information about the distribution of the refractive index (henceforth called Refractive Index Map (RIM)). This necessitates measuring deflections for several orientations of the object in order to recover the RIM. Sec. VI briefly describes how the sparsity of RIM helps in its reconstruction using deflections from only few orientations.

PS is supported by the DETROIT project (WIST3), Walloon Region, Belgium. LJ is supported by the Belgian FRS-FNRS fund.

[1] "Spread Spectrum" is not related to the studied deflection "spectrum" but it refers to the signal frequency spectrum.

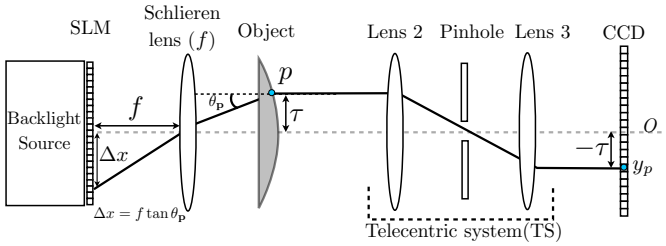

Fig. 2: A 2-D schematic of Schlieren deflectometer.

II. Schlieren Deflectometer

Deflection spectra can be measured by the Schlieren deflectometer, shown in Fig. 2, which consists of *(i)* a Spatial Light Modulator (SLM), *(ii)* the Schlieren lens with focal length f, *(iii)* the Telecentric System (TS) and *(iv)* the Charged Coupled Device (CCD) camera collecting the light.

The object to be analyzed is placed in between the Schlieren lens and the telecentric system. It is shined on its left by a light source and, due to the telecentric system, only the parallel light rays emerging out of the object are collected by the CCD. Moreover, up to a flip around the optical axis, each location $\boldsymbol{p}$ on the object at a distance τ from the optical axis O (dashed line), is probed by a corresponding CCD pixel also at a distance of τ from O. Each location $\boldsymbol{p}$ is thus in one-to-one correspondence with a CCD pixel and we will sometimes consider $\boldsymbol{p}$ as CCD pixel location.

From classical optics, a light ray that is incident on location $\boldsymbol{p}$ at an angle $\theta_{\boldsymbol{p}}$ originates from the light source at a distance of $\Delta x = f \tan\theta_{\boldsymbol{p}}$ from the optical axis. Likewise, the light rays originating at different locations on the source have different incident angles at $\boldsymbol{p}$. Since we can always virtually invert the light propagation in the system, everything works as if the object was shined on its right by a beam of parallel light rays. Therefore, up to a global scaling by f, the SLM plane is actually the local plane $\Pi_{\boldsymbol{p}}$ of the deflection spectrum occurring at $\boldsymbol{p}$. Modulating the SLM corresponds to modulating $s_{\boldsymbol{p}}$, while the light collected in CCD pixel $\boldsymbol{p}$ is just an inner product of $s_{\boldsymbol{p}}$ with the modulation.

If we generate M such modulations $\phi_i \in \mathbb{R}^N$ with $1 \le i \le M$ in the SLM of N pixels, considering the discrete nature of the CCD camera (having N_{C} pixels), the discretized deflection spectra are observed through

$$\boldsymbol{y}_k = \boldsymbol{\Phi}\boldsymbol{s}_k + \boldsymbol{n}, \quad 1 \le k \le N_{\mathrm{C}}, \tag{1}$$

where $\boldsymbol{\Phi}^T = (\boldsymbol{\phi}_1, \cdots, \boldsymbol{\phi}_M) \in \mathbb{R}^{N\times M}$ is the sensing matrix, k is a CCD pixel index, $\boldsymbol{s}_k \in \mathbb{R}^N$ is the discretized spectrum at the k^{th} pixel/object location, and $\boldsymbol{n}$ models the measurement noise (assumed Gaussian). Notice that the SLM and the CCD 2-D grids are represented as 1-D spaces for brevity of notation, so that $\boldsymbol{\Phi}$ is then a sensing 2-D matrix acting on 1-D vectors.

To optimize the design of $\boldsymbol{\Phi}$ we rely upon spread spectrum compressed sensing theory.

III. Spread Spectrum Compressive Sensing

In Spread Spectrum Compressive Sensing (SSCS), a signal $\boldsymbol{x} = \boldsymbol{\Psi}\boldsymbol{\alpha} \in \mathbb{C}^N$, having a *sparse* representation in an orthonormal *sparsity basis* $\boldsymbol{\Psi} \in \mathbb{C}^{N\times N}$, *i.e.*, $\|\boldsymbol{\alpha}\|_0 := \#\{j : \alpha_j \neq 0\} \le K \ll N$ is randomly pre-modulated before sensing [3]. Given a Rademacher or Steinhaus sequence $\boldsymbol{m} \in \mathbb{C}^N, |m_i| = 1$, the sensing process is summarized by

$$\boldsymbol{y} = \boldsymbol{\Gamma}_\Omega^* \boldsymbol{M}\boldsymbol{\Psi}\boldsymbol{\alpha} \ + \ \boldsymbol{n}, \tag{2}$$

where * denotes the conjugate transpose, $\boldsymbol{\Gamma} \in \mathbb{C}^{N\times N}$ is an orthonormal *sensing basis*, $\boldsymbol{\Gamma}_\Omega$ is the $M \times N$ submatrix formed by restricting the columns of $\boldsymbol{\Gamma}$ to those in $\Omega \subset [N] := \{1, \cdots, N\}$, $\boldsymbol{M} = \mathrm{diag}(\boldsymbol{m})$ and $\boldsymbol{n}$ is a Gaussian noise vector.

The signal is reconstructed by solving a convex optimization problem, known as Basis Pursuit De-Noising (BPDN) [5]

$$\widehat{\boldsymbol{\alpha}} := \underset{\widetilde{\boldsymbol{\alpha}}\in\mathbb{C}^N}{\arg\min} \ \|\widetilde{\boldsymbol{\alpha}}\|_1 \text{ subject to } \|\boldsymbol{y} - \boldsymbol{\Phi}\widetilde{\boldsymbol{\alpha}}\|_2 \le \epsilon, \tag{3}$$

where $\boldsymbol{\Phi} = \boldsymbol{\Gamma}_\Omega^* \boldsymbol{M}\boldsymbol{\Psi}$, and ϵ is a bound on $\|\boldsymbol{n}\|_2 \le \epsilon$.

For a given ϵ, the number of measurements M required by (3) to find a solution is, in general, governed by the sparsity level K and the *coherence*

$$\mu := \max_{1\le i,j\le N} |\langle \boldsymbol{\gamma}_i, \boldsymbol{M}\boldsymbol{\psi}_j \rangle|, \tag{4}$$

where $\boldsymbol{\gamma}_i$ and $\boldsymbol{\psi}_j$ are the columns of sensing and sparsity matrices respectively [3], [6]. Smaller the coherence, lesser is the number of measurements required for successful recovery of the solution, with a high probability.

Defining $C_{\boldsymbol{\Gamma},\boldsymbol{\Psi}} = \max_{1\le i,j\le N} \|\boldsymbol{\gamma}_i \circ \boldsymbol{\psi}_j\|_2$, where $\circ$ denotes pointwise product, the mutual coherence μ obeys

$$\mu \le C_{\boldsymbol{\Gamma},\boldsymbol{\Psi}} \sqrt{2\log(2N^2/\delta)}, \tag{5}$$

with probability at least $1 - \delta$. When $\boldsymbol{\Gamma}$ is a *universal basis*, *i.e.*, when all the entries have the same complex amplitude c, spread spectrum is optimal with $C_{\boldsymbol{\Gamma},\boldsymbol{\Psi}} = c$ and the coherence $\mu \simeq c$, with a very high probability, irrespective of the sparsity basis. Specifically, for Fourier and Hadamard bases, $\mu \simeq 1/\sqrt{N}$ with high probability. We see in next section how to exploit the spread spectrum CS method in our optical setup.

IV. Deflection Spectrum Reconstruction

To apply the ideas of spread spectrum CS to schlieren deflectometry, certain practical aspects have to be considered. Most importantly, as the Spatial Light Modulator (SLM) accepts only real and non-negative valued entries, we use the Hadamard (universal) basis $\boldsymbol{H}$ combined with a random Rademacher vector $\boldsymbol{m}$ with $m_i = \pm 1$ independently with equal probability for sensing.

Further, the sensing basis is biased to have all the entries non-negative and an extra measurement is obtained to remove the bias during reconstruction. The details about obtaining the measurements can be found in [7].

Noise estimation: If there is no test object, then by classical optics the measured deflection spectrum is constant in all CCD pixels and corresponds to a simple disk centered on the origin of the spectrum domain. We denote it as $\boldsymbol{s}^{\mathrm{no}}$. The disk diameter is proportional to the pinhole diameter of the system (see Fig. 2). This prior information aids us in calibrating the system and in estimating the noise level on the measurements.

From actual measurements in the absence of test object, we obtain, on an arbitrary CCD pixel, $\boldsymbol{y}^{\mathrm{no}} = \boldsymbol{\Phi}(\boldsymbol{s}^{\mathrm{no}} + \boldsymbol{n}_{\boldsymbol{s}}) + \boldsymbol{n}_{\boldsymbol{y}}$, where $\boldsymbol{n}_{\boldsymbol{s}}$ and $\boldsymbol{n}_{\boldsymbol{y}}$ are the unknown signal and observation noises. After a small calibration of the SLM origin, and up to

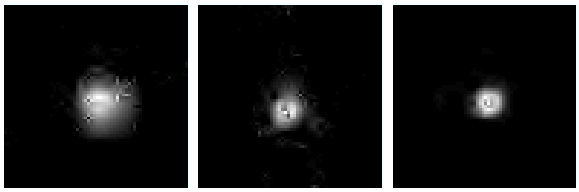

Fig. 3: An example of reconstruction using 2.5%, 10% and 100% of measurements.

a small optimization of the disk height in $\boldsymbol{s}^{\mathrm{no}}$, we can therefore compute a bound on the noise power as $\epsilon = \|\boldsymbol{\Phi}\boldsymbol{n_s} + \boldsymbol{n_y}\|_2 = \|\boldsymbol{y}^{\mathrm{no}} - \boldsymbol{\Phi}\boldsymbol{s}^{\mathrm{no}}\|_2$. We can either obtain this value for every M or estimate it for $M = N$ only and scale the result as $\epsilon(M) = \sqrt{M + 2\sqrt{M}}\ \epsilon(N)/\sqrt{N}$ for $M < N$. This estimate stems from the concentration properties of χ^2_M random variables.

Reconstruction procedure: For the reconstruction, we use the Daubechies 9/7 wavelet basis as our sparsity basis [8] which offers a sparser representation of the spectra than the canonical (Dirac) basis. To reconstruct the spectrum at any location k, an estimate of the sparse wavelet coefficients $\widehat{\boldsymbol{\alpha}}_k$ is obtained by solving (3) with the ϵ estimated above. The spectrum is then estimated by $\hat{\boldsymbol{s}}_k = \boldsymbol{\Psi}^* \widehat{\boldsymbol{\alpha}}_k$. To solve (3), we used the Chambolle-Pock algorithm, a first order primal-dual method for solving convex optimization problems using proximal operators [9]. Compared to a previous work on this subject [7], the reconstruction performance improved by constraining the estimate $\hat{\boldsymbol{s}}_k$ to be non-negative.

For evaluating compressive reconstruction performance, (3) was solved with $M = N$ measurements to obtain the reference reconstruction $\tilde{\boldsymbol{s}}_k$. Reconstructions for $M < N$ were compared with $\tilde{\boldsymbol{s}}_k$ using the (output) Signal-to-Noise Ratio oSNR $:= 20\log_{10}(\|\tilde{\boldsymbol{s}}_k\|_2/\|\tilde{\boldsymbol{s}}_k - \hat{\boldsymbol{s}}_k\|_2)$.

Experimental Results:[2] For experiments, we considered two plano convex lenses of optical powers 10.03D and 60D, and restricted the size of spectrum to 64×64 centered around the SLM origin, resulting in $N = 4096$. For 5 CCD locations, 10 independent reconstruction trials were performed for several values of M, by randomly drawing a new $\Omega \subset [N]$ every time.

Fig. 3 shows an example of deflection spectrum reconstructed using 2.5%, 10% and 100% of measurements, for the lens with $10D$ optical power. Note that the spectrum is well localized and sparse, corroborating our initial observation.

Fig. 4 shows the plot of oSNR versus the number of measurements M/N (in %), averaged over the trials and locations. The curves with square markers correspond to the solutions obtained using additional non-negativity constraints and the rest correspond to the lack of it. The oSNR improves as M/N increases, as expected. Though the absolute values of oSNR seem low, its significance has to be understood in the light of the input SNR, which is approximately computed as iSNR $:= 20\log_{10}(\|\boldsymbol{\Phi}\boldsymbol{s}^{\mathrm{no}}\|_2/\|\boldsymbol{y}^{\mathrm{no}} - \boldsymbol{\Phi}\boldsymbol{s}^{\mathrm{no}}\|_2) \simeq 4.34$ dB. The horizontal dotted line on the plot indicates the iSNR for our experiments, and it is clear that the reconstruction procedure improves the oSNR, beyond the iSNR, thereby demonstrating

[2]Computational resources have been provided by the supercomputing facilities of the Université catholique de Louvain (CISM/UCL) and the Consortium des Équipements de Calcul Intensif en Fédération Wallonie Bruxelles (CÉCI) funded by the F.R.S.-FNRS under convention 2.5020.11.

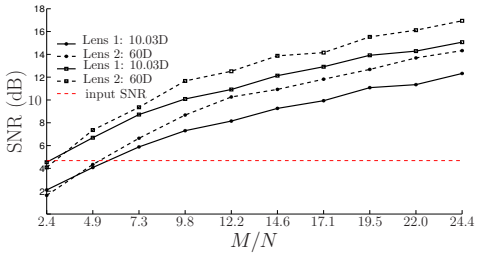

Fig. 4: Average reconstruction oSNR (in dB) as a function of M/N.

the ability of CS reconstruction of deflection spectra in low input SNR regime.

V. Obtaining Deflections without Reconstruction

Reconstruction of deflection spectra is a computationally intensive task and therefore if the objective is only to detect the location of the important feature of the spectrum (in our case, the location of the bright spot), then the idea of compressive domain signal processing can be used [10], [11]. Assuming that a template $\boldsymbol{g}^\rho$ for the feature can be built, the feature can be localized using a matched filtering operation performed directly on the measurements, without reconstructions. These locations provide a first guess of the deflections.

For *compressive spectrum detection*, given deflectometric measurements $\boldsymbol{y}_k$, we simply solve the following [7]

$$\widetilde{\tau}_k = \arg\max_{\tau} |\langle \boldsymbol{\Phi}^T \boldsymbol{y}_k, \boldsymbol{g}^\rho_\tau \rangle|, \tag{6}$$

where $\boldsymbol{g}^\rho_\tau$ is $\boldsymbol{g}^\rho$ translated by τ.

The experimental results showed that the distance between the centroids computed using compressive measurements and full reconstruction becomes sub-pixel for measurements size M/N as low as 4%, and continues to decrease as M increases. The evolution of the centroid estimation error versus the number of measurements M/N is available in [7].

We shall now see how to utilize deflection information for certain meaningful characterization of transparent objects.

VI. Refractive Index Map Reconstruction using Deflection Information

Characterizing a transparent object consisting of heterogeneous optical media by studying its Refractive Index Map (RIM), *i.e.*, the spatial distribution of the refractive index, is an important and challenging task for its manufacturing. In this section we will focus on the task of reconstructing RIM starting from deflection information.

The objective of the work is to demonstrate the relevance of sparsity and compressive sensing ideas for RIM reconstruction, independent of how the deflection maps are acquired (compressively or not). To emphasize that sparsity also helps in efficiently reconstructing RIM of transparent objects, we work with the deflection maps acquired (non-compressively) using the classical phase shifting schlieren method.

As shown in Fig. 5 (left), consider a refractive index map $\mathfrak{n}(\boldsymbol{r}), \boldsymbol{r} \in \mathbb{R}^2$ in the $\boldsymbol{e}_1\boldsymbol{e}_2$ plane (assuming that it is invariant along $\boldsymbol{e}_3$), that characterizes a complex object. For a given incident angle θ of the incoming light rays, schlieren deflectometer measures a two-dimensional map of the effective deflections $\Delta(\theta, \tau)$, where τ is the distance between the origin and the incident light ray under consideration.

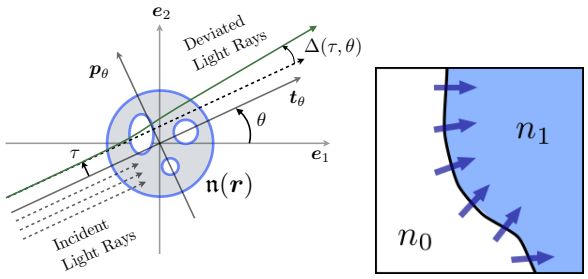

Fig. 5: (left) Model of light deflection through a transparent object. (right) TV model of RIM.

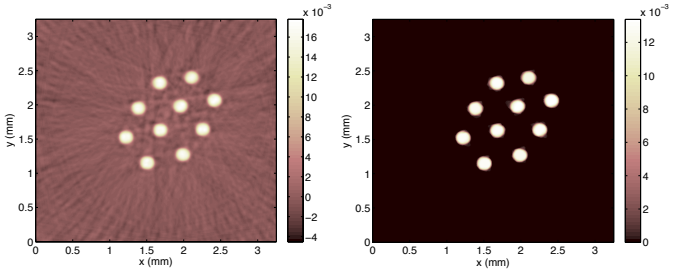

Fig. 6: An example of RIM reconstruction for a bundle of fibres with (left) the FBP and (right) TV minimization approach.

The measured deflection angles turn out to be the integral of the *transverse gradient* of the RIM, along the path of the light assumed to be straight (paraxial approximation) [12]. Notice that unlike the integration of the function itself in usual tomographic settings, here the integration is on the gradient of the function. Upon using the modified (deflectometric) Fourier slice theorem, the Fourier transform $\boldsymbol{y}_\theta$ of $\Delta(\theta,\tau)$, along τ for a fixed θ, provides one "slice" of the two-dimensional *polar* Fourier transform $\hat{\mathfrak{n}}(\boldsymbol{k})$ of $\mathfrak{n}(\boldsymbol{r})$ through the origin, *but each coefficient weighted by its distance to the frequency origin*. This weighting is in fact due to the integration of the gradient.

With a suitable discretization of the quantities and abuse of notations, the vectorized RIM $\mathfrak{n}$ and the vectorized Fourier transform of the deflection angles $\boldsymbol{y}_\theta$ are related by

$$\boldsymbol{y}_\theta = \boldsymbol{\Phi}\mathfrak{n} + \boldsymbol{n}, \tag{7}$$

where $\boldsymbol{\Phi}$ incorporates the Fourier operation and weighting factors arising from the slice theorem [13].

Reconstructing $\mathfrak{n}$ from the $\boldsymbol{y}_\theta$ involves measuring deflections from several incident angles θ and then solving an inverse problem using the forward model (7). To stabilize the inverse problem, suitable prior knowledge on $\mathfrak{n}$ has to be incorporated.

For a wide class of human made transparent objects, the RIM consists of slowly varying regions limited by sharp boundaries, as in Fig. 5(right), and therefore the RIM is sparse in the *gradient domain*. This prior knowledge about sparsity greatly helps us in reducing the number N_θ of incident angles that are needed to satisfactorily reconstruct the RIM.

Algorithmically, the RIM is reconstructed by promoting a solution with least Total Variation (TV) norm $\|\mathfrak{n}\|_{\text{TV}} = \|\nabla\mathfrak{n}\|_{2,1}$ [14], [9], that also respects the forward model (7) for a given noise level. The quality of the solution is further improved by using additional prior knowledge such as the non-negativity of $\mathfrak{n}$ and relevant boundary conditions.

For a test object of a bundle of optical fibres, Fig. 6(left) shows the reconstructed RIM, for the number of incident angles $N_\theta = 60$ (17% out of the possible 360 angles), using the well known Filtered Back Projection (FBP) algorithm that promotes a minimal ℓ_2 norm of the solution [15]. Fig. 6(right) shows the RIM reconstructed using a TV minimization approach, for the same number of angles. The TV reconstruction is better than that of FBP in not only suppressing the artifacts outside the fibre regions, but also in recovering the sharp edges between the fibres and the surroundings.

VII. Conclusions and Perspectives

This paper presents a novel approach for obtaining deflection information of transparent objects using schlieren deflectometer, and using this information to further characterize the objects. It has been demonstrated that suitable sparsity prior not only helps us to compressively acquire and reconstruct deflection maps, but also in efficiently using these deflections to reconstruct refractive index maps.

For further work, it is of foremost importance to understand the noise properties to tune the reconstruction method. Methods have to be developed to fully exploit the rich nature of deflection spectrum for object characterization. We also intend to develop approaches to exploit redundant dictionaries (e.g. undecimated wavelets), analysis-based reconstructions or correlation between neighbouring spectra for their simultaneous reconstruction.

References

[1] G. S. Settles, *Schlieren and Shadowgraph Techniques: Visualizing Phenomena in Transparent Media*. Springer, New York, NY, USA, 2001.

[2] L. Joannes, F. Dubois, and J. C. Legros, "Phase-shifting schlieren: high-resolution quantitative schlieren that uses the phase-shifting technique principle," *Applied optics*, vol. 42, no. 25, pp. 5046–5053, 2003.

[3] G. Puy, P. Vandergheynst, R. Gribonval, and Y. Wiaux, "Universal and efficient compressed sensing by spread spectrum and application to realistic fourier imaging techniques," *EURASIP Journal on Advances in Signal Processing*, vol. 2012, pp. 1–13, 2012.

[4] M. F. Duarte, M. A. Davenport, D. Takhar, J. N. Laska, T. Sun, K. F. Kelly, and R. G. Baraniuk, "Single-pixel imaging via compressive sampling," *IEEE Sig. Proc. Magazine*, vol. 25, no. 2, pp. 83–91, 2008.

[5] J. Tropp and S. Wright, "Computational methods for sparse solution of linear inverse problems," *Proceedings of the IEEE*, 2010.

[6] H. Rauhut, "Compressive sensing and structured random matrices," *Theoretical Found. and Num. Methods for Sparse Recovery*, 2010.

[7] P. Sudhakar, L. Jacques, X. Dubois, P. Antoine, and L. Joannes, "Compressive schlieren deflectometry," submitted to ICASSP 2013. [Online]. Available: http://arxiv.org/abs/1212.0433

[8] S. Mallat, *A Wavelet Tour of Signal Processing: The Sparse Way*, 3rd ed. Academic Press, 2008.

[9] A. Chambolle and T. Pock, "A first-order primal-dual algorithm for convex problems with applications to imaging," *Journal of Mathematical Imaging and Vision*, vol. 40, no. 1, pp. 120–145, May 2011.

[10] M. A. Davenport, M. F. Duarte, M. B. Wakin, J. N. Laska, D. Takhar, K. F. Kelly, and R. G. Baraniuk, "The smashed filter for compressive classification and target recognition," in *Proceedings of Computational Imaging V at SPIE Electronic Imaging*, San Jose, CA, Jan. 2007.

[11] M. A. Davenport, P. T. Boufounos, M. B. Wakin, and R. G. Baraniuk, "Signal processing with compressive measurements," *IEEE Journal on Selected Topics in Signal Processing*, vol. 4, no. 2, pp. 445–460, 2010.

[12] D. Beghuin, J.-L. Dewandel, L. Joannes, E. Foumouo, and P. Antoine, "Optical deflection tomography with the phase-shifting schlieren," *Optics letters*, vol. 35, no. 22, pp. 3745–3747, 2010.

[13] A. Gonzalez, L. Jacques, C. D. Vleeschouwer, and P. Antoine, "Compressive optical deflectometric tomography: A constrained total-variation minimization approach," *CoRR*, vol. abs/1209.0654, 2012.

[14] L. I. Rudin, S. Osher, and E. Fatemi, "Nonlinear total variation based noise removal algorithms," *Phys. D*, vol. 60, pp. 259–268, Nov. 1992.

[15] *Principles of computerized tomographic imaging*. Philadelphia, PA, USA: Society for Industrial and Applied Mathematics, 2001.